Hyperbolic Non-Abelian Semimetal

Tarun Tummuru,[1,*] Anffany Chen,[2,*] Patrick M. Lenggenhager,[1,3,4,5,*]
Titus Neupert,[1] Joseph Maciejko,[2,6] and Tomáš Bzdušek[1,3,†]

[1]*Department of Physics, University of Zurich, Winterthurerstrasse 190, 8057 Zurich, Switzerland*
[2]*Department of Physics & Theoretical Physics Institute, University of Alberta, Edmonton, Alberta T6G 2E1, Canada*
[3]*Condensed Matter Theory Group, Paul Scherrer Institute, 5232 Villigen PSI, Switzerland*
[4]*Institute for Theoretical Physics, ETH Zurich, 8093 Zurich, Switzerland*
[5]*Max Planck Institute for the Physics of Complex Systems, Nöthnitzer Str. 38, 01187 Dresden, Germany*
[6]*Quantum Horizons Alberta, University of Alberta, Edmonton, Alberta T6G 2E1, Canada*

(Received 3 August 2023; revised 29 February 2024; accepted 28 March 2024; published 14 May 2024)

We extend the notion of topologically protected semi-metallic band crossings to hyperbolic lattices in a negatively curved plane. Because of their distinct translation group structure, such lattices are associated with a high-dimensional reciprocal space. In addition, they support non-Abelian Bloch states which, unlike conventional Bloch states, acquire a matrix-valued Bloch factor under lattice translations. Combining diverse numerical and analytical approaches, we uncover an unconventional scaling in the density of states at low energies, and illuminate a nodal manifold of codimension five in the reciprocal space. The nodal manifold is topologically protected by a nonzero second Chern number, reminiscent of the characterization of Weyl nodes by the first Chern number.

DOI: 10.1103/PhysRevLett.132.206601

Introduction.—Topological semimetals are gapless electronic phases with stable band-touching points at the Fermi energy. As solid-state analogs of relativistic fermions, low-energy excitations in semimetals are often imbued with nontrivial topological properties. Dirac and Weyl semimetals in three dimensions, for instance, exhibit a range of intriguing properties such as protected surface states, anomalous Hall effect, chiral anomaly, and unusual magneto-resistance [1–8]. Broadly, semimetals can be categorized based on spatial dimension, origin of band crossings, and properties of the nodal manifold (e.g., its degeneracy and codimension) [9]. All existing models and material realizations, however, are typically embedded in geometrically flat Euclidean space.

Hyperbolic lattices—regular tessellations of 2D hyperbolic space with constant negative curvature [10]—provide the means to study quantum matter in non-Euclidean geometry. Recent realizations in coplanar waveguide resonators [11] and topoelectrical circuits [12–15] have catalyzed the research of physical properties of hyperbolic lattices. Theoretical studies of hyperbolic analogs of topological insulators [14–20] show that bulk topological invariants and protected edge modes persist in hyperbolic space. Other celebrated condensed-matter phenomena such as Hofstadter spectra [21,22], flat bands [23–26], higher-order topology [27–29], strong correlations [30–33], and fractons [34,35] have also been explored in the hyperbolic context.

Hyperbolic lattices have unique features that unlock new physics beyond the Euclidean paradigm. Hyperbolic

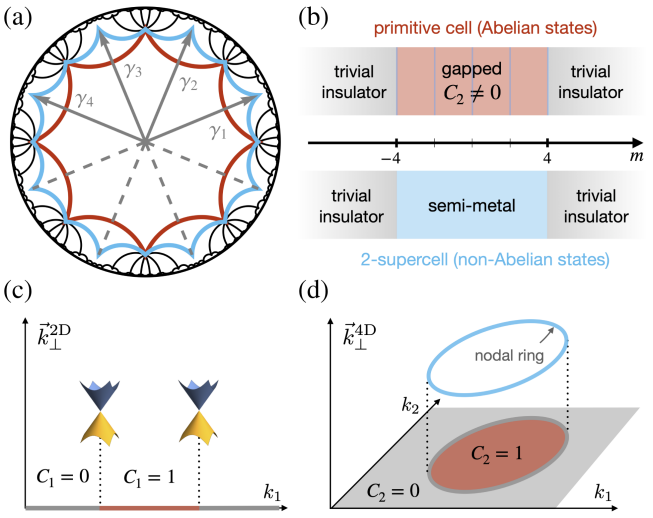

FIG. 1. Real- and reciprocal-space structure of the hyperbolic non-Abelian semimetal. (a) The model is defined on the {8,8} lattice, displayed in the Poincaré disk model, wherein the single- and two-site unit cells are marked in red and blue, respectively. Translation generators of the primitive cell are denoted by γ_j. (b) Unit cell size affects the accessible reciprocal space and, consequently, the phase diagram for $|m| < 4$: the primitive cell suggests topological insulator phases with Chern numbers $|C_2| = 1$ or 3, whereas the 2-supercell description exhibits a topological semimetal. (c) Comparison to Weyl semimetals, where 2D planes (along $\vec{k}_\perp^{2D}$) between the Weyl nodes have a finite first Chern number. (d) Similarly, in the hyperbolic semimetal, when $|m| \in (3,4)$, a nodal ring separates 4D orthogonal subspaces (along $\vec{k}_\perp^{4D}$) with a nontrivial second Chern number.

translation groups, known as Fuchsians, are non-Abelian [36]. Accordingly, their unitary irreducible representations (IRs) can have a dimension d larger than one. Via a generalized Bloch theorem, hyperbolic band theory (HBT) [37,38] provides a reciprocal-space description of hyperbolic lattices and their eigenstates. Hyperbolic Bloch states are classified as Abelian [U(1)] [37] or non-Abelian [U(d) for $d > 1$] [38,39] depending on the rank d of the matrix-valued Bloch factor acquired under lattice translations. Whereas U(1) eigenstates are labeled by a vector analogous to crystal momentum, additional quantum numbers are required to distinguish U(d) Bloch states. The problem of accessing and characterizing non-Abelian Bloch states constitutes an actively investigated topic [40–43].

In this work, we present a hyperbolic lattice model whose semimetallic topology is inherently rooted in non-Abelian Bloch states. While the Abelian spectrum is gapped, we demonstrate the presence of a topologically protected nodal manifold in the non-Abelian U(2) Bloch bands, which results in a gapless density of states (DOS). Summarized in Fig. 1, this nodal manifold in reciprocal space is associated with a finite second Chern number C_2. There is no Euclidean analog of such a phase because 2D Euclidean lattices admit neither non-Abelian Bloch states nor a second Chern number. We term this phase a *hyperbolic non-Abelian semimetal*.

Model.—HBT suggests a way to translate higher-dimensional Euclidean models to the hyperbolic plane. The mapping is especially lucid for 4D Euclidean Hamiltonians because of a one-to-one correspondence between the Euclidean BZ and the simplest [i.e., the U(1)/Abelian] hyperbolic BZ of the {8,8} lattice—the hyperbolic lattice where eight regular octagons meet at each vertex. Motivated by this connection, we study the hyperbolic counterpart of the 4D quantum Hall insulator (QHI).

Conventionally, the 4D Euclidean QHI is defined by a Dirac tight-binding model on the hypercubic lattice [44,45]:

$$\mathcal{H} = \sum_{r,j}\left[\psi_r^\dagger \frac{\mathbb{\Gamma}_5 - \mathrm{i}\mathbb{\Gamma}_j}{2}\psi_{r+j} + \mathrm{h.c.}\right] + m\sum_r \psi_r^\dagger \mathbb{\Gamma}_5 \psi_r, \quad (1)$$

where $\{\mathbb{\Gamma}_\mu\}_{\mu=1}^5$ denote the Dirac matrices, $\{\mathbb{\Gamma}_\mu, \mathbb{\Gamma}_\nu\} = 2\delta_{\mu\nu}\mathbb{1}$. In terms of the Pauli matrices σ_i, the choice $\{\mathbb{\Gamma}_\mu\}_{\mu=1}^5 = \{\sigma_1\sigma_0, \sigma_2\sigma_0, \sigma_3\sigma_1, \sigma_3\sigma_2, \sigma_3\sigma_3\}$ ensures that $\mathbb{\Gamma}_\mu$ is real (imaginary) for μ odd (even). The four components of the spinor ψ_r correspond to internal degrees of freedom at site $r \in \mathbb{Z}^4$, and $j = 1, \ldots, 4$ label orthogonal directions.

The {8,8} hyperbolic lattice, illustrated in Fig. 1(a), provides a convenient setting to reinterpret the above model [15]. Formally, the lattice is defined by its Fuchsian group Γ, an infinite translation group with four noncommuting

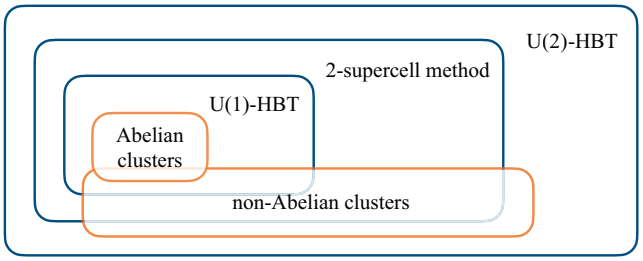

FIG. 2. Schematic summary of techniques used in this work to access eigenstates of hyperbolic lattices. Orange (blue) indicates real- (reciprocal-)space methods.

generators γ_j [arrows in Fig. 1(a)] that obey a single constraint [37]:

$$\Gamma = \langle \gamma_1, \gamma_2, \gamma_3, \gamma_4 | \gamma_1\gamma_2^{-1}\gamma_3\gamma_4^{-1}\gamma_1^{-1}\gamma_2\gamma_3^{-1}\gamma_4 = 1 \rangle. \quad (2)$$

The "hyperbolized" 4D QHI Hamiltonian is realized with the following reinterpretation: r is the unit cell position on the hyperbolic plane and $r + j$ denotes a cell shifted by the translation operator γ_j.

To obtain a reciprocal-space perspective, we proceed in two steps. First, as in the Euclidean case, the lattice needs to be compactified, i.e., periodic boundary conditions (PBC) are imposed and edges of the unit cell related by translation symmetry are identified, producing a surface of genus $\mathfrak{g} \geq 2$ [37]. Unlike the Euclidean case, choosing an enlarged n-site unit cell ($n > 1$) increases the genus [43]. Second, one has to choose a d-dimensional IR D_λ of the translation group, where λ labels a point in a $[2d^2(\mathfrak{g}-1)+2]$-dimensional space of d-dimensional IRs of Γ [38]. A generic Bloch Hamiltonian $H_\lambda^{(n,d)}$ thus obtained determines states in the Brillouin zone $\mathrm{BZ}^{(n,d)}$. The integers n and d provide two handles to access different sectors of the hyperbolic reciprocal space.

On the {8,8} lattice, the smallest unit cell ($n = 1$ or primitive cell) is given by the red octagon in Fig. 1(a). It compactifies to a $\mathfrak{g} = 2$ surface when the opposite edges are identified. Further, in U(1) representations, λ are the crystal momenta whose components correspond to the four non-contractible cycles of the genus-2 surface. The mapping $D_\lambda(\gamma_j) = D_{\boldsymbol{k}}(\gamma_j) = \mathrm{e}^{\mathrm{i}k_j}$ satisfies the constraint in Eq. (2) and defines the U(1) Bloch Hamiltonian

$$H_{\boldsymbol{k}}^{(1,1)} = \sum_\mu d_{\boldsymbol{k}}^\mu \mathbb{\Gamma}_\mu, \quad (3)$$

with $d_{\boldsymbol{k}}^\mu = (\sin k_1, \sin k_2, \sin k_3, \sin k_4, m_{\boldsymbol{k}})$ and $m_{\boldsymbol{k}} = m + \sum_j \cos k_j$. Evidently, these expressions are equivalent to the Fourier transform of the Hamiltonian in Eq. (1), such that U(1)-HBT reproduces results from the 4D Euclidean case: at half-filling, the model undergoes topological phase transitions at $|m| = 0, 2, 4$, but is gapped otherwise with a nonvanishing C_2 [45], as depicted in Fig. 1(b).

The corresponding gapped DOS for $m = 3$ is plotted with the red curve in Fig. 3(a).

However, as foreshadowed earlier, one should also account for $d > 1$ IRs of Γ. We first demonstrate the existence of "in-gap" states by real-space diagonalization on PBC clusters, and then show that these states originate from non-Abelian reciprocal space using U(2)-HBT and the supercell method (Fig. 2).

PBC clusters.—Closed hyperbolic lattices formed by pairing open edges of a finite-sized lattice are termed PBC clusters [46]. Efficient construction of large PBC clusters can be achieved through computational methods in geometric group theory [47]. Depending on the particular edge pairing, PBC clusters can be classified into two categories: Abelian or non-Abelian [38]. In Abelian clusters, the non-Abelian hyperbolic translation group Γ modulo the edge pairing becomes Abelian. In other words, the translation generators effectively commute on Abelian clusters, so the wavefunctions of a translationally invariant Hamiltonian must be 1D IRs of the translation group in Eq. (2). Here, we exclusively consider non-Abelian PBC clusters as we are interested in higher-dimensional IRs arising from the noncommutativity of the generators, which are necessary to approximate the thermodynamic limit [40–43]. We numerically diagonalize the hyperbolized Hamiltonian (1) on 13 non-Abelian {8,8} PBC clusters, with the number of primitive cells ranging from 300 to 1800. The resulting DOS averaged over these clusters for $m = 3$ is depicted by the black curve in Fig. 3(a). Our first main finding is the discovery of states within the gap of the Abelian Bloch states.

$U(d)$-HBT.—To demonstrate that these in-gap states can be attributed to non-Abelian Bloch physics, we first describe the corresponding BZs [56]. Here, the Bloch states transform in representations $D_\lambda(\gamma_j) = U_j e^{ik_j}$, where $\boldsymbol{U} = \{U_j\}_{j=1}^4 \in \mathrm{SU}(d)$ are special unitary $(d \times d)$ matrices that satisfy Eq. (2). The specification of λ requires $2d^2 + 2$ parameters, of which four may be understood as hyperbolic momenta $\boldsymbol{k} = \{k_j\}_{j=1}^4$ and the remaining $2d^2 - 2$ characterize $\boldsymbol{U}$. Focusing on a single primitive cell ($n = 1$), the states in $\mathrm{BZ}^{(1,d)}$ can be described by the non-Abelian Bloch Hamiltonian

$$H_\lambda^{(1,d)} = \sum_j \left[\left(\frac{\mathbb{\Gamma}_5 - i\mathbb{\Gamma}_j}{2} \right) \otimes D_\lambda(\gamma_j) + \mathrm{h.c.} \right] + m(\mathbb{\Gamma}_5 \otimes \mathbb{1}_d). \tag{4}$$

Although an explicit parametrization of $\mathrm{BZ}^{(1,d)}$ is currently lacking, one may randomly sample the subspace of $\mathrm{SU}(d)$ matrices that obey Eq. (2) using a procedure described in [47]. For different choices of $\boldsymbol{U}$ and $\boldsymbol{k}$, a numerical diagonalization of $H_\lambda^{(1,d)}$ allows for a reconstruction of the $\mathrm{U}(d)$ spectra. We here focus on the simplest nontrivial case $d = 2$, since spectra of small systems that could be realized in experiments are dominated by low-dimensional representations [38]. The DOS thus obtained is plotted in yellow in Fig. 3(a). Consistent with our exact diagonalization results on PBC clusters, non-Abelian states fill the band gap of the Abelian spectrum.

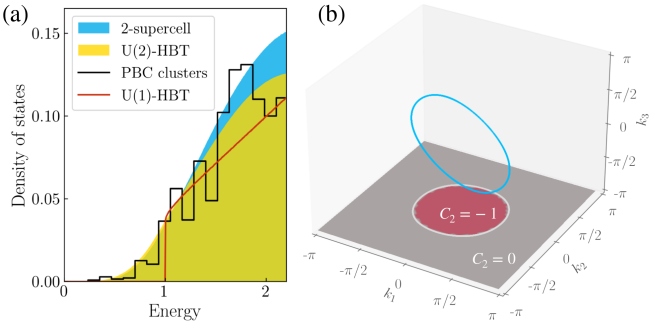

FIG. 3. Hyperbolic non-Abelian semimetal with Dirac mass $m = 3$. (a) Energy spectra computed with various numerical approaches (cf. Fig. 2). In contrast to the hard gap predicted by U(1)-HBT, the other approaches indicate a semimetallic DOS symmetric about zero energy. (b) Low-energy excitations are manifested by a nodal ring in the 2-supercell description. Numerically obtained nodes in the 6D $\mathrm{BZ}^{(2,1)}$ have been projected to the first three momentum components. Projection onto the first two coordinates appears as the white curve. Computing the second Chern number C_2 as a function of (k_1, k_2) shows that 4D subspaces passing through the ring are topological.

Supercell method.—An alternative way to access non-Abelian Bloch states is the supercell method [43]. Instead of tessellating the infinite lattice with copies of the primitive cell [red octagon in Fig. 1(a)], the lattice is subdivided into collections of $n > 1$ primitive cells, called *n-supercells* [blue polygon in Fig. 1(a) depicts the 2-supercell]. Copies of the primitive cell covering the lattice are related by elements of the full translation group of the lattice $\Gamma^{(1)} = \Gamma$, while copies of an n-supercell are related only by elements of an index-n normal subgroup $\Gamma^{(n)} \lhd \Gamma^{(1)}$.

In either case, translation symmetry allows a single-cell description of the infinite system by going to hyperbolic reciprocal space as described previously. In Euclidean lattices, enlarging the unit cell introduces band folding and a reduction in BZ size while the total number of states remains constant. In contrast, in hyperbolic lattices, the decomposition of reciprocal space into the generalized BZs is changed: The BZs for the primitive cell $\mathrm{BZ}^{(1,d)}$ are different from the ones for an n-supercell, $\mathrm{BZ}^{(n,d)}$. Nevertheless, their union (over IR dimensions d) is expected to remain the same, such that both are descriptions of the same infinite system. Specifically, as a consequence of the negative curvature, the genus $\mathfrak{g}$ of the compactified manifold (and thereby the dimension of $\mathrm{BZ}^{(n,1)}$ which is a $2\mathfrak{g}$-dimensional torus), grows linearly with the supercell

size. In particular, $\mathrm{BZ}^{(1,1)}$ is 4D, while $\mathrm{BZ}^{(2,1)}$ is 6D, with $\mathrm{BZ}^{(1,1)}$ passing through the center of $\mathrm{BZ}^{(2,1)}$ [47].

The advantage of working with supercells comes from the fact that, in contrast to the non-Abelian BZs, the U(1)-BZs are well understood and an explicit parametrization in terms of Bloch phase factors is known. Because of $\Gamma^{(n)}$ being an index-n subgroup of $\Gamma^{(1)}$, U(1) representations of $\Gamma^{(n)}$ induce $\mathrm{U}(n)$ representations of $\Gamma^{(1)}$, which are either reducible or irreducible [43]. Due to the growing dimension of $\mathrm{BZ}^{(n,1)}$ with supercell size n, most of the $\mathrm{U}(n)$ representations of $\Gamma^{(1)}$ are non-Abelian, i.e., they do not split into a product of U(1) representations. Therefore, by applying U(1)-HBT to larger supercells, more non-Abelian states are captured.

We focus again on the simplest nontrivial case of 2-supercell, thus gaining access to certain non-Abelian U(2) Bloch states. We utilize the HyperCells package for GAP [57–59] and the HyperBloch package for *Mathematica* [60], to sample states in $\mathrm{BZ}^{(2,1)}$. The result, plotted in blue in Fig. 3(a), confirms our earlier findings: a semimetallic DOS within the gap of the Abelian Bloch states.

Nodal ring.—In unison, the three methods paint a clear picture: While the U(1) spectrum is gapped, non-Abelian Bloch states arise inside the gap. Since the three DOS curves in Fig. 3(b) match each other near zero energy, we use the 2-supercell approach to derive an approximate low-energy theory by studying the Bloch Hamiltonian $H_{\boldsymbol{k}}^{(2,1)}$ analytically for $|m| \gtrsim 3$. We find that its zero-energy eigenstates form a *nodal ring* inside $\mathrm{BZ}^{(2,1)}$ whose projection onto a 3D subspace is shown in Fig. 3(b). This nodal ring is protected by space-time-inversion symmetry [47]. Through a basis change of the Hamiltonian, linear transformation of the momentum space from $\boldsymbol{k}$ to $\boldsymbol{q}$, and a Taylor expansion around the origin [47], we find that the spectral gap vanishes when

$$q_1^2 + q_2^2 = 6(4 - |m|) \quad \text{and} \quad q_3 = q_4 = q_5 = q_6 = 0. \tag{5}$$

As a circle with mass-dependent radius, the nodal manifold shrinks to a point at the topological phase transitions $|m| = 4$.

To understand the nodal topology, it is useful to draw parallels with Weyl semimetals in 3D Euclidean space. Weyl nodes can be understood as sources and sinks of Berry curvature in momentum space. As a consequence of the dipolar configuration, a 2D plane situated between two nodes of opposite charge experiences a net Berry flux and features a finite Chern number, cf. Fig. 1(c). In a similar spirit, one may expect the nodal ring in 6D hyperbolic reciprocal space to encode nontrivial topology. Since our starting point was the 4D QHI, the second Chern number C_2 [61] is the relevant topological quantity. Indeed, integration over the four momenta $k_{3,\ldots,6}$ shows that the nodal ring projection to the (k_1, k_2) plane encloses a region where $C_2 = -1$, as shown in Fig. 3(b).

While the DOS of 3D Weyl semimetals near $E = 0$ scales as $\rho(E) \propto E^2$ [2], we expect that for the hyperbolic non-Abelian semimetal it scales as $\rho(E) \propto E^4$. To see this, first observe that 4D QHI Hamiltonian $\mathcal{H}$ carries a spinful space-time-inversion symmetry, $\mathcal{PT} = \mathbb{\Gamma}_2\mathbb{\Gamma}_4\mathcal{K}$ with $(\mathcal{PT})^2 = -\mathbb{1}$ and complex conjugation $\mathcal{K}$. We find [47] that the $\mathcal{PT}$ symmetry is inherited by the 2-supercell Bloch Hamiltonian $H_{\boldsymbol{k}}^{(2,1)}$. It follows from the von Neumann–Wigner theorem [62,63] that $H_{\boldsymbol{k}}^{(2,1)}$ generically exhibits band nodes of codimension $\mathfrak{d} = 5$, consistent with the observed nodal ring of dimension $\dim[\mathrm{BZ}^{(2,1)}] - \mathfrak{d} = (6 - 5) = 1$. Assuming the most generic scenario where the bands disperse linearly in the five directions perpendicular ($\perp$) to the nodal ring, quartic DOS scaling $\rho(E) = \int \mathrm{d}^5 k_\perp \delta(E - v|k_\perp|) \propto E^4$ follows. Through numerical analysis [47], we find that within the 2-supercell approximation for $|m| \in (0, 4)$ the DOS scales as $\rho(E) \propto E^\alpha$ with $\alpha \in (3.3, 4.1)$. Specifically for $m \in (3, 4)$, where a single nodal ring is present, we confirm the predicted value $\alpha = 4$ within the numerical precision.

Experimental signatures.—A priori, any physical realization of a hyperbolic lattice has states that transform under higher-dimensional IRs. To experimentally probe non-Abelian states, however, one needs to isolate them from the U(1) states. The hyperbolic non-Abelian semimetal provides an energy window to *exclusively* access these states. In coplanar waveguide resonators [11], for instance, a gap would appear as a dip in the transmission spectra, whereas a finite DOS at low energies would support transmission.

To understand the physical implications of nodal topology, recall the case of Weyl semimetals. There, each 2D slice between the Weyl nodes, carrying nonzero value of C_1 [cf. Fig. 1(c)], contributes to anomalous Hall conductance $\sigma_{xy} = (e^2/2\pi h)\Delta k$ where Δk is the momentum node separation [2–4]. Similarly, the response of the hyperbolic non-Abelian semimetal to external fields should be contingent on the nodal manifold geometry. We therefore study the second Chern number C_2^{cl} in small PBC clusters (consisting of N primitive cells), which is generated by filled states under flux insertion $(\mathbb{\Gamma}_5 - i\mathbb{\Gamma}_j) \mapsto (\mathbb{\Gamma}_5 - i\mathbb{\Gamma}_j)e^{i\phi_j}$ with $\boldsymbol{\phi} \in [0, 2\pi)^{\times 4}$ in Eq. (1) [47]. Practically, such phase manipulation can be implemented with tunable complex-phase elements [12] in topoelectrical circuits [13–15], where the eigenstates necessary for computing C_2^{cl} can be accessed with simple oscilloscope measurements. For Abelian states, the flux insertion induces a momentum shift $\boldsymbol{k} \mapsto \boldsymbol{k} + \boldsymbol{\phi}$; therefore, all eigenstates contribute equally to the integration, implying $C_2^{\mathrm{cl}}/N = C_2$. In contrast, the trajectory of non-Abelian states under flux insertion may fall outside the nodal-ring manifold [cf. Fig. 3(b)], or pass through an additional nodal

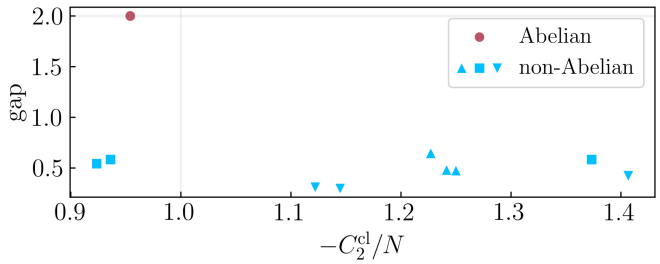

FIG. 4. Flux insertion in PBC clusters. We study Abelian and non-Abelian clusters with $N = 16, 18, 20$ (up-pointing triangle, square, down-pointing triangle) primitive cells and use a phase space grid of 20^4 to compute the cluster-specific second Chern number C_2^{cl} with $m = 3$. While the Abelian clusters agree with U(1)-HBT, non-Abelian clusters show smaller gaps owing to the semimetallic states and C_2^{cl}/N has a larger variance.

manifold not represented in the 6D $\mathrm{BZ}^{(2,1)}$. In both cases, one anticipates deviation from the linear scaling $C_2^{\mathrm{cl}} = NC_2$. Figure 4 (supplemented with further data in [47]) shows the result of such integration for randomly selected Abelian (red) and non-Abelian (blue) clusters, revealing agreement with our theoretical arguments. We leave the study of the convergence of C_2^{cl}/N in the thermodynamic limit [40–43] to future works.

Conclusion and outlooks.—Semimetals are fertile platforms that emulate particle physics models on one hand and actualize solid-state notions of topology on the other. Conventionally, they have been studied in Euclidean space. Extending the notion of topological band nodes to negatively curved space, we investigated the hyperbolized 4D QHI Hamiltonian. The model exhibits striking features that have no counterpart in Euclidean crystals, such as band nodes stabilized by a second Chern number and low-energy excitations transforming exclusively in non-Abelian IRs of the hyperbolic translation group.

Our findings motivate broader and more systematic studies of band topology in hyperbolic lattices. In particular, the semimetallic nature of the hyperbolized QHI model inspires the search for *fully gapped* hyperbolic topological insulators in which the region with a finite second Chern number [red in Fig. 3(b)] spans the entire higher-dimensional BZ [20]. Furthermore, while the U(1) and U(2) representations considered here dominate the spectra of small systems that can be realized in experiments [38], higher-dimensional U(d) representations are necessary to describe the system in the thermodynamic limit [40–43]. Our preliminary data obtained for larger n-supercells [47] suggest not only a change in the DOS scaling exponent α but also a gradual evolution of the non-Abelian semimetal below (above) a critical value $|m_c| \simeq 2.5$ to a non-Abelian metal (insulator) phase.

On the experimental front, to probe the transport associated with C_2 [44], one needs to reconcile a dimensionality mismatch: the hyperbolic plane is two-dimensional, whereas four orthogonal directions enter (via the four-component Levi-Civita symbol) the nonlinear response to applied fields [45,64]. Experimental realizations would also benefit from a generalization of the hyperbolic non-Abelian semimetal to $\{p, q\}$ lattices with a smaller curvature per site than the {8,8} lattice assumed here. Furthermore, to enhance the versatility of experimental realizations, it is desirable to seek implementations of hyperbolic lattices in other analog simulators including silicon photonics [65], as well as in quantum platforms such as optical tweezer arrays [66,67] and trapped ions [68]. In a broader context, exciting open questions arise for hyperbolic topological models in relation to the bulk-boundary correspondence [16–18] and the holographic principle [69–72].

The code and the generated data used to arrive at the conclusions presented in this work are publicly available in Ref. [73].

We would like to thank I. Boettcher and R. Thomale for valuable discussions and the referees for their insightful questions. T. T. and T. N. acknowledge funding from the European Research Council (ERC) under the European Union's Horizon 2020 research and innovation programm (ERC-StG-Neupert-757867-PARATOP). A. C. was supported by the University of Alberta startup fund UOFAB Startup Boettcher and the Avadh Bhatia Fellowship. J. M. was supported by NSERC Discovery Grants No. RGPIN-2020-06999 and No. RGPAS-2020-00064; the Canada Research Chair (CRC) Program; the Government of Alberta's Major Innovation Fund (MIF); the Tri-Agency New Frontiers in Research Fund (NFRF, Exploration Stream); and the Pacific Institute for the Mathematical Sciences (PIMS) Collaborative Research Group program. P. M. L. and T. B. were supported by the Ambizione Grant No. 185806 by the Swiss National Science Foundation (SNSF). T. B. was supported by the Starting Grant No. 211310 by SNSF. P. M. L. acknowledges funding by the European Union (ERC, QuSimCtrl, 101113633). Views and opinions expressed are, however, those of the authors only and do not necessarily reflect those of the European Union or the European Research Council Executive Agency. Neither the European Union nor the granting authority can be held responsible for them.

*These authors contributed equally to this letter.
†tomas.bzdusek@uzh.ch

[1] X. Wan, A. M. Turner, A. Vishwanath, and S. Y. Savrasov, Topological semimetal and Fermi-arc surface states in the electronic structure of pyrochlore iridates, Phys. Rev. B **83**, 205101 (2011).

[2] A. A. Zyuzin and A. A. Burkov, Topological response in Weyl semimetals and the chiral anomaly, Phys. Rev. B **86**, 115133 (2012).

[3] P. Hosur and X. Qi, Recent developments in transport phenomena in Weyl semimetals, C.R. Phys. **14**, 857 (2013).
[4] A. A. Burkov, Anomalous Hall effect in Weyl metals, Phys. Rev. Lett. **113**, 187202 (2014).
[5] M. M. Vazifeh and M. Franz, Electromagnetic response of Weyl semimetals, Phys. Rev. Lett. **111**, 027201 (2013).
[6] O. Vafek and A. Vishwanath, Dirac fermions in solids: From high-T_c cuprates and graphene to topological insulators and Weyl semimetals, Annu. Rev. Condens. Matter Phys. **5**, 83 (2014).
[7] N. P. Armitage, E. J. Mele, and A. Vishwanath, Weyl and Dirac semimetals in three-dimensional solids, Rev. Mod. Phys. **90**, 015001 (2018).
[8] N. P. Ong and S. Liang, Experimental signatures of the chiral anomaly in Dirac-Weyl semimetals, Nat. Rev. Phys. **3**, 394 (2021).
[9] H. Gao, J. W. Venderbos, Y. Kim, and A. M. Rappe, Topological semimetals from first principles, Annu. Rev. Mater. Sci. **49**, 153 (2019).
[10] H. S. M. Coxeter, Crystal symmetry and its generalizations, Proc. Trans. R. Soc. Can. **51**, 1 (1957).
[11] A. J. Kollár, M. Fitzpatrick, and A. A. Houck, Hyperbolic lattices in circuit quantum electrodynamics, Nature (London) **571**, 45 (2019).
[12] A. Chen, H. Brand, T. Helbig, T. Hofmann, S. Imhof, A. Fritzsche, T. Kießling, A. Stegmaier, L. K. Upreti, T. Neupert, T. Bzdušek, M. Greiter, R. Thomale, and I. Boettcher, Hyperbolic matter in electrical circuits with tunable complex phases, Nat. Commun. **14**, 622 (2023).
[13] P. M. Lenggenhager, A. Stegmaier, L. K. Upreti, T. Hofmann, T. Helbig, A. Vollhardt, M. Greiter, C. H. Lee, S. Imhof, H. Brand, T. Kießling, I. Boettcher, T. Neupert, R. Thomale, and T. Bzdušek, Simulating hyperbolic space on a circuit board, Nat. Commun. **13**, 4373 (2022).
[14] W. Zhang, H. Yuan, N. Sun, H. Sun, and X. Zhang, Observation of novel topological states in hyperbolic lattices, Nat. Commun. **13**, 2937 (2022).
[15] W. Zhang, F. Di, X. Zheng, H. Sun, and X. Zhang, Hyperbolic band topology with non-trivial second Chern numbers, Nat. Commun. **14**, 1083 (2023).
[16] S. Yu, X. Piao, and N. Park, Topological hyperbolic lattices, Phys. Rev. Lett. **125**, 053901 (2020).
[17] D. M. Urwyler, P. M. Lenggenhager, I. Boettcher, R. Thomale, T. Neupert, and T. Bzdušek, Hyperbolic topological band insulators, Phys. Rev. Lett. **129**, 246402 (2022).
[18] Z.-R. Liu, C.-B. Hua, T. Peng, and B. Zhou, Chern insulator in a hyperbolic lattice, Phys. Rev. B **105**, 245301 (2022).
[19] Q. Pei, H. Yuan, W. Zhang, and X. Zhang, Engineering boundary-dominated topological states in defective hyperbolic lattices, Phys. Rev. B **107**, 165145 (2023).
[20] A. Chen, Y. Guan, P. M. Lenggenhager, J. Maciejko, I. Boettcher, and T. Bzdušek, Symmetry and topology of hyperbolic Haldane models, Phys. Rev. B **108**, 085114 (2023).
[21] K. Ikeda, S. Aoki, and Y. Matsuki, Hyperbolic band theory under magnetic field and Dirac cones on a higher genus surface, J. Phys. Condens. Matter **33**, 485602 (2021).
[22] A. Stegmaier, L. K. Upreti, R. Thomale, and I. Boettcher, Universality of Hofstadter butterflies on hyperbolic lattices, Phys. Rev. Lett. **128**, 166402 (2022).
[23] A. J. Kollár, M. Fitzpatrick, P. Sarnak, and A. A. Houck, Line-graph lattices: Euclidean and non-Euclidean flat bands, and implementations in circuit quantum electrodynamics, Commun. Math. Phys. **376**, 1909 (2020).
[24] A. Saa, E. Miranda, and F. Rouxinol, Higher-dimensional Euclidean and non-Euclidean structures in planar circuit quantum electrodynamics, arXiv:2108.08854.
[25] T. Bzdušek and J. Maciejko, Flat bands and band-touching from real-space topology in hyperbolic lattices, Phys. Rev. B **106**, 155146 (2022).
[26] R. Mosseri, R. Vogeler, and J. Vidal, Aharonov-Bohm cages, flat bands, and gap labeling in hyperbolic tilings, Phys. Rev. B **106**, 155120 (2022).
[27] Z.-R. Liu, C.-B. Hua, T. Peng, R. Chen, and B. Zhou, Higher-order topological insulators in hyperbolic lattices, Phys. Rev. B **107**, 125302 (2023).
[28] Y.-L. Tao and Y. Xu, Higher-order topological hyperbolic lattices, Phys. Rev. B **107**, 184201 (2023).
[29] J. Sun, C.-A. Li, S. Feng, and H. Guo, Hybrid higher-order skin-topological effect in hyperbolic lattices, Phys. Rev. B **108**, 075122 (2023).
[30] X. Zhu, J. Guo, N. P. Breuckmann, H. Guo, and S. Feng, Quantum phase transitions of interacting bosons on hyperbolic lattices, J. Phys. Condens. Matter **33**, 335602 (2021).
[31] P. Bienias, I. Boettcher, R. Belyansky, A. J. Kollár, and A. V. Gorshkov, Circuit quantum electrodynamics in hyperbolic space: From photon bound states to frustrated spin models, Phys. Rev. Lett. **128**, 013601 (2022).
[32] N. Gluscevich, A. Samanta, S. Manna, and B. Roy, Dynamic mass generation on two-dimensional electronic hyperbolic lattices, arXiv:2302.04864.
[33] N. Gluscevich and B. Roy, Magnetic catalysis in weakly interacting hyperbolic Dirac materials, arXiv:2305.11174.
[34] H. Yan, Hyperbolic fracton model, subsystem symmetry, and holography, Phys. Rev. B **99**, 155126 (2019).
[35] H. Yan, K. Slagle, and A. H. Nevidomskyy, Y-cube model and fractal structure of subdimensional particles on hyperbolic lattices, arXiv:2211.15829.
[36] I. Boettcher, A. V. Gorshkov, A. J. Kollár, J. Maciejko, S. Rayan, and R. Thomale, Crystallography of hyperbolic lattices, Phys. Rev. B **105**, 125118 (2022).
[37] J. Maciejko and S. Rayan, Hyperbolic band theory, Sci. Adv. **7**, abe9170 (2021).
[38] J. Maciejko and S. Rayan, Automorphic Bloch theorems for hyperbolic lattices, Proc. Natl. Acad. Sci. U.S.A. **119**, e2116869119 (2022).
[39] N. Cheng, F. Serafin, J. McInerney, Z. Rocklin, K. Sun, and X. Mao, Band theory and boundary modes of high-dimensional representations of infinite hyperbolic lattices, Phys. Rev. Lett. **129**, 088002 (2022).
[40] F. R. Lux and E. Prodan, Spectral and combinatorial aspects of Cayley-Crystals, Ann. Henri Poincaré (2023).
[41] F. R. Lux and E. Prodan, Converging periodic boundary conditions and detection of topological gaps on regular hyperbolic tessellations, Phys. Rev. Lett. **131**, 176603 (2023).

[42] R. Mosseri and J. Vidal, Density of states of tight-binding models in the hyperbolic plane, Phys. Rev. B **108**, 035154 (2023).
[43] P. M. Lenggenhager, J. Maciejko, and T. Bzdušek, Non-Abelian hyperbolic band theory from supercells, Phys. Rev. Lett. **131**, 226401 (2023).
[44] S.-C. Zhang and J. Hu, A four-dimensional generalization of the quantum Hall effect, Science **294**, 823 (2001).
[45] X.-L. Qi, T. L. Hughes, and S.-C. Zhang, Topological field theory of time-reversal invariant insulators, Phys. Rev. B **78**, 195424 (2008).
[46] F. Sausset and G. Tarjus, Periodic boundary conditions on the pseudosphere, J. Phys. A **40**, 12873 (2007).
[47] See Supplemental Material at http://link.aps.org/supplemental/10.1103/PhysRevLett.132.206601, which cites additional Refs. [48–55] for further details on PBC clusters (construction and flux threading), U(d)-HBT, and the supercell method (2-supercell Hamiltonian, symmetry analysis, mass dependence of the nodal manifold, larger n-supercell spectra).
[48] F. Rober, The GAP package LINS (2020), https://github.com/FriedrichRober/LINS.
[49] D. Firth, An algorithm to find normal subgroups of a finitely presented group, up to a given finite index, Ph.D. thesis, University of Warwick, 2004.
[50] D. J. S. Robinson, *A Course in the Theory of Groups*, 2nd ed. (Springer, New York, 1996).
[51] T. Fukui, Y. Hatsugai, and H. Suzuki, Chern numbers in discretized Brillouin zone: Efficient method of computing (spin) Hall conductances, J. Phys. Soc. Jpn. **74**, 1674 (2005).
[52] Á. Nagy and S. Rayan, On the hyperbolic Bloch transform, Ann. Henri Poincaré **25** (2023).
[53] J. B. Bronzan, Parametrization of $SU(3)$, Phys. Rev. D **38**, 1994 (1988).
[54] R. Miranda, *Algebraic Curves and Riemann Surfaces* (American Mathematical Society, Providence, 1995).
[55] S. Ryu, A. P. Schnyder, A. Furusaki, and A. W. W. Ludwig, Topological insulators and superconductors: Tenfold way and dimensional hierarchy, New J. Phys. **12**, 065010 (2010).
[56] G. Shankar and J. Maciejko, Hyperbolic lattices and two-dimensional Yang-Mills theory, arXiv:2309.03857.
[57] P. M. Lenggenhager, J. Maciejko, and T. Bzdušek, HyperCells: A GAP package for constructing primitive cells and supercells of hyperbolic lattices (2023), https://github.com/patrick-lenggenhager/HyperCells.
[58] M. Conder, Quotients of triangle groups acting on surfaces of genus 2 to 101 (2007).
[59] GAP, GAP—groups, algorithms, and programming, version 4.11.1, The GAP Group (2021).
[60] P. M. Lenggenhager, J. Maciejko, and T. Bzdušek, HyperBloch: A Mathematica package for hyperbolic tight-binding models and the supercell method (2023), https://github.com/patrick-lenggenhager/HyperBloch.
[61] M. Mochol-Grzelak, A. Dauphin, A. Celi, and M. Lewenstein, Efficient algorithm to compute the second Chern number in four dimensional systems, Quantum Sci. Technol. **4**, 014009 (2018).
[62] J. von Neumann and E. Wigner, Über das verhalten von eigenwerten bei adiabatischen prozessen, Phys. Z. **30**, 465 (1929).
[63] T. Bzdušek and M. Sigrist, Robust doubly charged nodal lines and nodal surfaces in centrosymmetric systems, Phys. Rev. B **96**, 155105 (2017).
[64] H. M. Price, O. Zilberberg, T. Ozawa, I. Carusotto, and N. Goldman, Four-dimensional quantum Hall effect with ultracold atoms, Phys. Rev. Lett. **115**, 195303 (2015).
[65] L. Huang, L. He, W. Zhang, H. Zhang, D. Liu, X. Feng, F. Liu, K. Cui, Y. Huang, W. Zhang, and X. Zhang, Hyperbolic photonic topological insulators, arXiv:2401.16006.
[66] A. M. Kaufman and K.-K. Ni, Quantum science with optical tweezer arrays of ultracold atoms and molecules, Nat. Phys. **17**, 1324 (2021).
[67] B. M. Spar, E. Guardado-Sanchez, S. Chi, Z. Z. Yan, and W. S. Bakr, Realization of a Fermi-Hubbard optical tweezer array, Phys. Rev. Lett. **128**, 223202 (2022).
[68] C. Monroe, W. C. Campbell, L.-M. Duan, Z.-X. Gong, A. V. Gorshkov, P. W. Hess, R. Islam, K. Kim, N. M. Linke, G. Pagano, P. Richerme, C. Senko, and N. Y. Yao, Programmable quantum simulations of spin systems with trapped ions, Rev. Mod. Phys. **93**, 025001 (2021).
[69] E. Witten, Anti-de Sitter space and holography, Adv. Theor. Math. Phys. **2**, 253 (1998).
[70] J. Zaanen, Y.-W. Sun, Y. Liu, and K. Schalm, *Holographic Duality in Condensed Matter Physics* (Cambridge University Press, Cambridge, England, 2015).
[71] M. Asaduzzaman, S. Catterall, J. Hubisz, R. Nelson, and J. Unmuth-Yockey, Holography on tessellations of hyperbolic space, Phys. Rev. D **102**, 034511 (2020).
[72] J. Chen, F. Chen, Y. Yang, L. Yang, Z. Chen, Y. Meng, B. Yan, X. Xi, Z. Zhu, G.-G. Liu, P. P. Shum, H. Chen, R.-G. Cai, R.-Q. Yang, Y. Yang, and Z. Gao, Ads/CFT correspondence in hyperbolic lattices, arXiv:2305.04862.
[73] T. Tummuru, A. Chen, P. M. Lenggenhager, T. Neupert, J. Maciejko, and T. Bzdušek, Supplementary data and code for hyperbolic non-Abelian semimetal (2023), 10.5281/zenodo.10729119.